

# Background-oriented schlieren diagnostics for large-scale explosive testing

M. J. Hargather

Received: 22 June 2012 / Revised: 24 February 2013 / Accepted: 18 April 2013  
© Springer-Verlag Berlin Heidelberg 2013

**Abstract** Experimental measurements of shock wave propagation from explosions of C4 are presented. Each test is recorded with a high-speed digital video camera and the shock wave is visualized using background-oriented schlieren (BOS). Two different processing techniques for BOS analysis are presented: image subtraction and image correlation. The image subtraction technique is found to provide higher resolution for identifying the location of a shock wave propagating into still air. The image correlation technique is more appropriate for identifying shock reflections and multiple shock impacts in a region with complex flow patterns. The optical shock propagation measurements are used to predict the peak overpressure and overpressure duration at different locations and are compared to experimental pressure gage measurements. The overpressure predictions agree well with the pressure gage measurements and the overpressure duration prediction is within an order of magnitude of the experimental measurements. The BOS technique is shown to be an important tool for explosive research which can be simply incorporated into typical large-scale outdoor tests.

**Keywords** Explosive characterization · Background-oriented schlieren · Blast testing

## 1 Introduction

Testing of explosives and energetic materials has benefited significantly from high-speed digital imaging technology. Modern high-speed digital cameras have almost entirely replaced traditional film cameras and are widely used for studying explosive events. The majority of the high-speed imaging that is done, however, is only used to image explosion processes, and few attempts are made to apply modern digital schlieren techniques to the visualization of the associated compressible phenomena.

### 1.1 Explosive testing background

Much of the research and testing related to explosives has used photography as an important source of data and evaluation, as exemplified by the atomic bomb tests [1]. Many classic research investigations placed an emphasis on obtaining measurements of shock wave locations from photo records and refractive techniques or smoke-particle tracers [2–4]. Modern large-scale explosives research relies heavily on high-speed photography, but rarely includes refractive measurements of shock wave propagation, with a few notable exceptions. Clarke et al. [5] applied refractive imaging to measure detonator performance and Steward et al. [6] used optical techniques to characterize large-caliber muzzle blast waves. Sommersel et al. [7] and Mizukaki et al. [8] applied background-oriented schlieren (BOS) techniques to measure shock propagations from explosions.

In the laboratory, several researchers have applied refractive imaging techniques to the study of explosions. In particular, the work by Kleine et al. [9] demonstrated the advantage of using small-scale explosive charges and refractive imaging to obtain detailed characterizations of explosions. Other

---

Communicated by H. Kleine.

---

M. J. Hargather (✉)  
Department of Mechanical Engineering, New Mexico Tech,  
801 Leroy Place, Socorro, NM 87801, USA  
e-mail: mjh@nmt.edu

researchers have built upon these techniques and applied them to studying a range of explosive phenomena [10–12].

The present work expands upon the work of Sommersel et al. [7] and Mizukaki et al. [8] with the application of two different BOS processing techniques to measure shock propagation to determine incident overpressure, overpressure duration, and to identify shock reflections in a confined geometry.

## 1.2 Background-oriented schlieren

The background-oriented schlieren technique was developed almost simultaneously by Meier [13] and Dalziel et al. [14]. The technique requires only a simple background with intensity variations, a camera, and a computer. Two high-resolution images of the background, one with a refractive disturbance and one without, are processed with a computer routine to identify distortions of the background due to the refractive disturbance. The basic geometry of a BOS system is shown in Fig. 1. A single light–dark boundary is shown as the background, but typically a background with many randomly distributed light–dark boundaries is used. The present work uses a “natural” background of a hillside with randomly distributed and shaped bushes, trees, and rocks which provide the light–dark boundaries, which has been used by many others [7, 8, 15, 16]. The simplicity of BOS and its ability to produce quantitative measurements has made it an increasingly used technique in aerodynamics and fluid dynamics research, but has seen little use in energetic materials research. Quantitative measurements from BOS have been presented by Dalziel et al. [17], and many others [18–20].

The “sensitivity” of the BOS system can be defined as the smallest light refraction angle  $\epsilon$  that can be visualized. In general, the sensitivity is maximized by minimizing the ratio  $t/L$ , maximizing the distance  $L$ , and maximizing the camera pixel resolution [13, 18, 20]. The constraints include maintaining the “schlieren object” in reasonable focus and maintaining the background in sharp focus. The current work maximizes sensitivity with  $t/L \approx 0.5$ , as given in Fig. 2. The high-speed digital camera used here limits the camera resolution to  $<1$  megapixel.

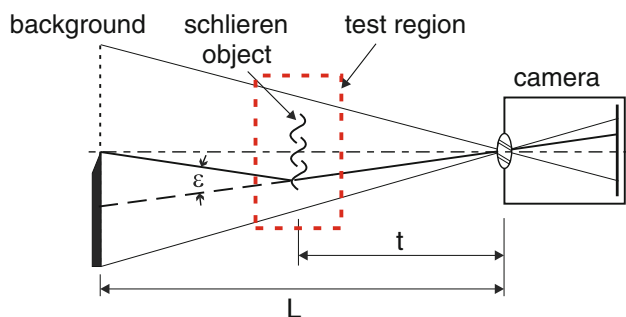


**Fig. 1** Schematic of the typical optical arrangement for BOS imaging

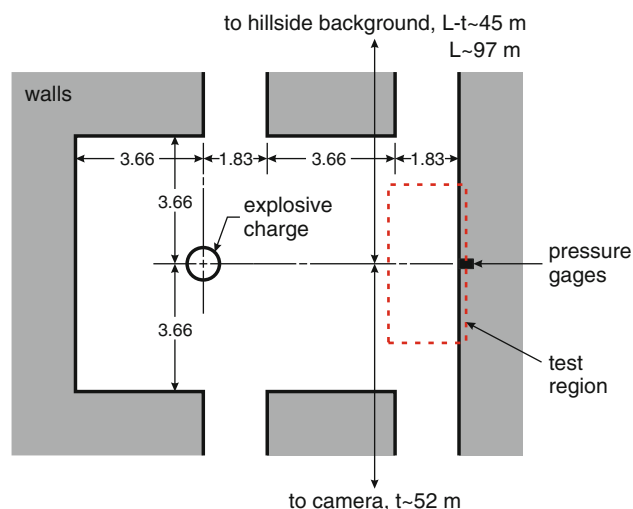


**Fig. 2** Schematic of the experimental setup with dimensions in meters. The two pressure gages were flush-mounted on the wall as indicated and were stacked vertically, 2.43 m apart. The charges were placed 0.69 m off the ground, even with the lower pressure gage (gage 1)

The BOS technique is used here to provide refractive imaging with a large field of view in an outdoor test environment. The visualization of such a large field with other refractive techniques would require large optical components or screens, which are not always amenable to outdoor testing [21]. The simplicity of BOS and the ability to use natural backgrounds makes it a natural fit for use in outdoor environments.

## 2 Experimental methods

These experiments were performed at the Energetic Materials Research and Testing Center (EMRTC) at New Mexico Tech. The experiments used C4 explosive charges initiated with an RP-83 detonator. The high-speed digital images were recorded with a Phantom v611 camera, which was triggered by the detonator initiation system. A summary of the two experiments is given in Table 1.

### 2.1 Experimental setup

The experiments were performed at a test site with a fixed geometry as shown schematically in Fig. 2. The solid wall structures were 7.3-m tall and made of concrete. The explosive charges were placed at the location shown in Fig. 2. The distance from the ground to the center of each charge was 0.69 m.

The pressure gages [model 102A06 from PCB, 500 psi (3,447 kPa) range] were flush mounted in the wall shown in Fig. 2. Data from two gages are used: gage 1 at the same height as the explosive charge centerline, and gage 2 located

**Table 1** Experimental conditions

Test	C4 mass (kg)	Camera frame rate (fps)	Frame size (pixels)	Image resolution (pixels per m)
1	4.54	10,000	1,280 × 456	81.2
2	27.22	15,000	464 × 704	196

2.43 m above gage 1 on the same wall (shown in Fig. 3). Each gage was sampled at 500 kHz with a PCB signal conditioner and data acquisition system using PXI 6133 cards. The manufacturer voltage-to-pressure calibration for each gage was used.

The relative camera-to-charge and camera-to-background distances are important for BOS “sensitivity” (Sect. 1.2), but do not need to be precisely measured because quantitative density measurements are not being obtained [18,20]. The camera is sharply focused on the background [16,20], but due to limited depth of field, the walls in the “test region” are slightly out of focus. Pixel-to-physical-distance calibrations were performed in the test region, in line with the explosive centerline and are given in Table 1. The defocusing in the test region contributed to the experimental uncertainty of the calibrations and is accounted for in the measurement uncertainty of  $\pm 1$  pixel for all measurements.

The high-speed camera recorded the tests at the frame rates and frame sizes specified in Table 1. The image resolution increased for test 2 because a greater camera zoom was used to image a more limited field of view; only the region outlined in Fig. 3b was imaged in test 2.

For each test, the natural BOS background had to be imaged with sufficient contrast to allow each processing method to identify unique features. Using sunlight illumination, the required contrast was obtained by imaging each test with the maximum shutter speed, equal to the inverse of the frame rate. These exposure times are considered long for

explosive experiments and result in “smearing” of the shock (observed in Fig. 8). For the shock position measurement, the long exposure does not have any effect. The leading edge observed is the shock position at the end of each frame exposure. The shock velocity is calculated from the shock position in sequential frames, divided by the time between images, given by the camera frame rate. The long exposure prevented quantitative density measurements due to smearing of the shock. A short enough exposure time was unattainable here with sunlight illumination. Other illumination sources such as argon bombs or flash lamps could have been used, but were not attempted here. The long exposure time was deemed acceptable because the focus of this effort was to measure shock propagation characteristics. Future work will perform quantitative BOS measurements of the density field produced by explosions and will explore supplemental illumination.

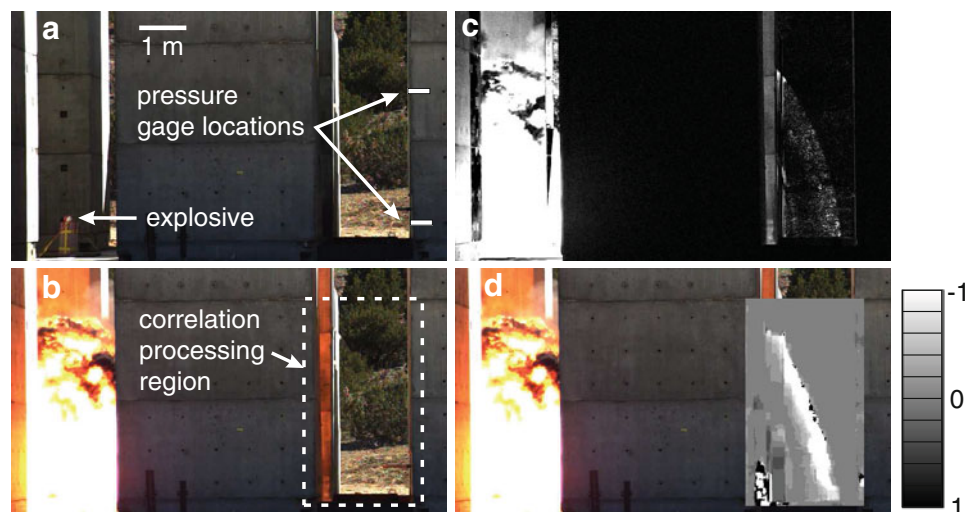
## 2.2 Background-oriented schlieren processing

Two methods of BOS processing were used in this work: image subtraction and image correlation. Both methods analyze individual frames of the high-speed video relative to a “tare” image recorded before the explosion. Each image after the explosion is considered a “flow” image. The tare image and a flow image for test 1 are shown in Fig. 3a, b, respectively.

The image subtraction method identifies locations, where the pixel intensity changed between the two images [16]. The tare image is subtracted from each flow image using MATLAB and a pixel-by-pixel routine that creates the new processed image with a new intensity at each pixel location  $(i, j)$  according to:

$$\text{new}(i, j) = \frac{(\text{flow}(i, j) - \text{tare}(i, j))^2}{\frac{\text{flow}(i, j) + \text{tare}(i, j)}{2} + 1} \quad (1)$$

**Fig. 3** **a** Tare image for test 1, **b** flow image 9 ms after the explosion, **c** image created from image subtraction of **a** and **b**, **d** contours showing horizontal pixel shift as measured from the image correlation between **a** and **b**



As shown in Fig. 3c, this method clearly reveals the shock location due to its distortion of the background. The grayscale intensity is related to the magnitude of the pixel intensity change between the two images. This method does not provide information on how a pixel intensity changed; the intensity change could be due to motion within the image, light intensity variation (common in explosive research), or the presence of a refractive disturbance.

The image correlation method uses a cross-correlation between the tare and flow images. This is the traditional method for analyzing BOS images [13, 15, 18] and results in the measurement of a “pixel shift” between the images. The magnitude of the pixel shift is related to the magnitude of the density gradient and the direction indicates the density gradient sign. The pixel shift is a quantitative measurement of the density field [17, 19, 20], but it is used here only to identify the shock wave leading edge and propagation direction.

The image correlation is calculated using the MATLAB function *normxcorr2*, and a routine written by the author [16].  $20 \times 20$  correlation windows are used and the correlation is performed for each pixel in the image. This is not typical, but is required here to accurately capture the leading edge of the shock.

The horizontal pixel shift calculated by the correlation is contour-plotted with a grayscale intensity to provide a “schlieren-like” image and overlaid on the original image in Fig. 3d. This plot is optically equivalent to a vertical knife-edge schlieren image [16]. The negative pixel shift indicates that the light is bent toward the left in the image, as expected for a shock wave propagating to the right. Only the area shown in Fig. 3b is processed with the correlation method.

The green plane of each red–green–blue (RGB) image was used for both processing methods. The green plane was chosen because it is centered in the visible spectrum and contained the greatest pixel intensities. It was also used because there are more green pixels in the camera’s Bayer filter. A Bayer filter is a color filter array which is used to obtain color images from a monochromatic sensor [22]. The filter is patterned with red, green, and blue filters which allow individual colors to expose individual pixels. The filter has 25 % red, 50 % green, and 25 % blue pixels, arranged in a repeating square pattern. The red, green, and blue values at the other pixel locations are calculated with a demosaicking algorithm [22]. The demosaicking did not contribute to the uncertainty of the shock position measurement because a large region of the visible shock wave was used to define the position, instead of using a single point.

For the image subtraction processing, converting the RGB image to a grayscale image, then processing it added noise due to pixel intensity variations between color planes between images (influenced by the Bayer filter demosaicking). For the correlation method, no differences were observed for performing the correlation on each color channel individually,

on the color image, or on a grayscale image created from the color image. The color correlation and grayscale routines were rejected because they were slower than processing a single channel.

### 3 Experimental results

The experiments performed here were analyzed to measure shock Mach numbers using the two BOS techniques. The optically measured Mach numbers were used to determine the peak reflected pressure and overpressure duration at the pressure gage locations, and were compared to the gage measurements. The BOS images were also used to correlate the gage-recorded pressure–time histories to subsequent shock impingements on the gages.

#### 3.1 Shock wave propagation measurement

The BOS images from the background subtraction procedure were used to measure the shock position as a function of time in the experiments. The position of the shock leading edge and its distance from the charge center was identified for each image. Sachs’ scaling [3, 23] was applied to scale the results to a 1 kg charge at normal temperature and pressure ( $T = 288.16$  K,  $P = 101,325$  Pa) [9, 11]. The measured, scaled shock radius as a function of scaled time is given in Fig. 4. The data from the two tests were collected over the same range of physical radii from the charge, but when scaled the data provides information across two different distance ranges because the tests had different mass explosive charges. The primary shock wave propagation was unaffected by any reflections within the test geometry. Also no Mach stem was observed in any test.

For ease of manipulation and to provide a general relationship for shock radius versus time, the scaled data are fit using a least-squares regression to the equation proposed by Dewey [3, 9]:

$$R_S = A + Ba_0t_S + C\ln(1 + a_0t_S) + D\sqrt{\ln(1 + a_0t_S)} \quad (2)$$

where  $a_0$  is the speed of sound in the scaled conditions. In addition to the measured shock radius data, an additional point of the shock radius being located at the explosive charge radius at time  $t_S = 0$  was included to improve the curve fit [3]. From this fit, the coefficients  $A$ ,  $B$ ,  $C$ , and  $D$  provide a unique characterization of the shock radius versus time for a given explosive. The coefficient  $B$  is forced to 1 here to provide a shock wave velocity asymptote to the speed of sound [3]. The coefficients for C4 from this data are:  $A = 0.010656$ ,  $B = 1$ ,  $C = -0.48533$ ,  $D = 2.7577$ .

The shock Mach number as a function of radius is calculated and plotted in Fig. 5. The experimental Mach number is calculated from a centered finite difference on each frame.

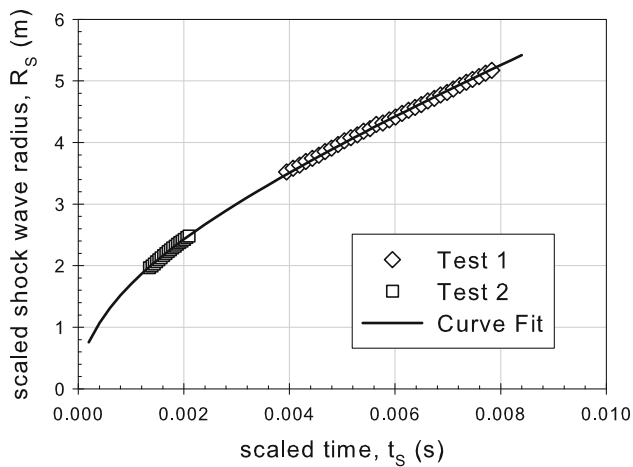


**Fig. 4** Measured shock radius as a function of time, in scaled coordinates. The error in the experimental data is smaller than the symbol size

The curve fit Mach number is determined from a differentiation of (2) with respect to time. This shock Mach number versus radius profile is a more unique and detailed characterization of an explosive than other typical measurements like “TNT equivalence” [9, 11], and is superior to other characterization approaches that simply scale curve fits, such as the Kingery–Bullmash equation to approximate a specific explosive.

The uncertainty in the shock radius is approximately  $\pm 1$  pixel. The uncertainty in Mach number is  $< \pm 0.1$  and is due to the pixel resolution of the images. The pixel resolution also results in the finite Mach number increments of the experimental data. Improving the pixel resolution would

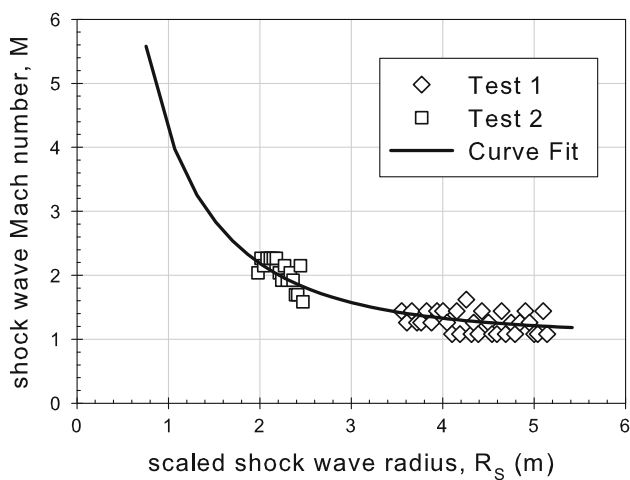


**Fig. 5** Mach number versus scaled radius for C4 showing both experimental data and the curve fit representation of the data. The error in measured radius is less than the symbol size. The error in measured Mach number is approximately two times the symbol size

decrease the error in position and Mach number. The error in time measurement is negligible.

Although only two experiments were performed, the test-to-test repeatability of these measurements is expected to be within the experimental error of an individual measurement because the C4 detonation process is highly repeatable. Some test-to-test variability is expected due to anomalies such as small fragments produced, but tracking of the primary shock wave is expected to be highly repeatable for C4. More experimental data, however, should be collected to improve the curve fit and establish a standard for C4. Performing more measurements was outside the present scope of work, but will be pursued in the future.

### 3.2 Pressure measurement

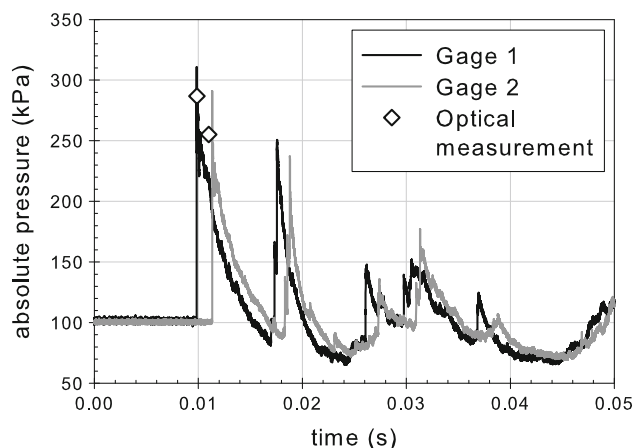
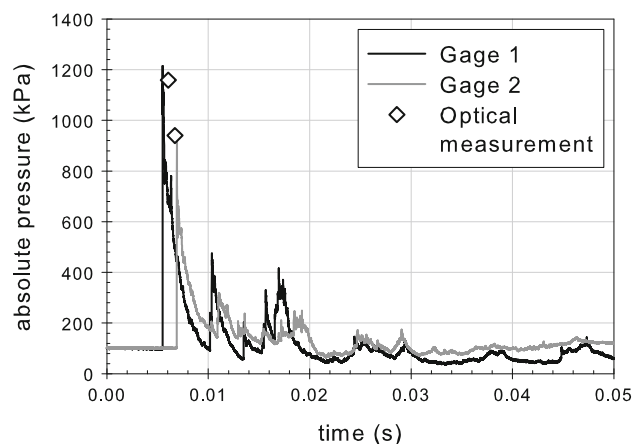
One goal of the BOS measurement was to determine the peak overpressure from the shock Mach number [23] and to compare the measured peak overpressure. Pressure as a function of time was measured at two different gages during these experiments. Pressure gage 1 observes a near normal shock wave impingement and reflection in both tests. The shock wave Mach number at the gage location is measured directly, and is presented in Table 2. The Mach number is used to obtain the peak reflected pressure [23], which is given in Table 2 and shown graphically in Figs. 6 and 7 along with the measured pressure–time histories.

Figures 6 and 7 also show the pressure–time histories for gage 2, located 2.43 m above gage 1. The shock on gage 2 is not normal, but rather an oblique reflection. The pressure behind the oblique reflection is calculated using gas dynamic oblique–shock relationships [23], assuming the shock wave is planar and the angle of incidence is known. The shock wave incidence angle is approximated from the horizontal and vertical distances between the charge center and the gage; for gage 2 the angle is approximately  $18.2^\circ$ . The angle was also measured via a manual inspection of the BOS images, and the two agreed within  $\pm 2\%$ .

The optically measured peak overpressure for both the normal and oblique shock reflections agree well with the pressure gage measurements. The optical measurements underpredict the peak gage pressures. This underprediction may actually be the result of pressure gage overshoot in response to the shock impingement [23]. The experimental error on the optical pressure measurements is significantly larger than the error on the pressure gages (with the exception of pressure gage overshoot). The uncertainty in the optical measurements is ultimately due to pixel resolution limitations. The optical measurement uncertainty can be reduced through the use of the curve fit, but more experimental data is desired to significantly reduce the uncertainty. Although the optical measurements have a large uncertainty, they help to

**Table 2** Optical and pressure gage measurement summary

Test	Gage #	Mach number	Peak pressure		Overpressure duration	
			Optical (kPa)	Gage (kPa)	Gage (ms)	Prediction (ms)
1	1	$1.27 \pm 0.09$	$288 \pm 40$	$311 \pm 1$	5.29	4.37
1	2	$1.24 \pm 0.09$	$255 \pm 40$	$291 \pm 1$	5.41	4.52
2	1	$1.85 \pm 0.05$	$1,160 \pm 50$	$1,215 \pm 1$	4.61	4.44
2	2	$1.76 \pm 0.05$	$940 \pm 50$	$951 \pm 1$	–	4.91

**Fig. 6** Measured pressure as a function of time for test 1 at pressure gage locations 1 and 2. The optical measurements are shown as the data symbols and are positioned at the time recorded, measured by the camera frame rate. The optical measurements have an error of approximately  $\pm 40$  kPa**Fig. 7** Measured pressure as a function of time for test 2 at pressure gage locations 1 and 2. The optical measurements are shown as the data symbols and are positioned at the time recorded, measured by the camera frame rate. The optical measurements have an error of approximately  $\pm 50$  kPa

build confidence in the gage measurements and demonstrate the advantages of incorporating optical imaging.

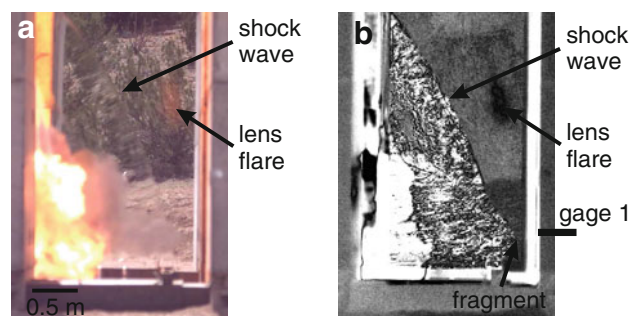
The optical measurements also have some error in the time of arrival of the shock waves, specifically for gage 1 in test

2 (Fig. 7). Upon inspection of the high-speed video, a fragment is observed impacting the wall near the pressure gage ahead of the primary shock wave (Fig. 8). This fragment was ignored in the shock position tracking, thus the optical data predicts the pressure peak slightly after the observed pressure peak. From the high-speed video, the fragment impacts approximately six frames (0.4 ms) before the primary shock wave would have impacted, which is approximately equal to the time offset between the optical and pressure gage data in Fig. 7. The error is thus not in the optical prediction, but an anomaly in the experiment that would not be observed without optical visualization.

Other slight variations in the time of arrival are due to pixel resolution uncertainty and could be reduced with more experiments and a better curve fit.

### 3.3 Overpressure duration measurement

The overpressure duration, which is important for defining explosive impulse [23], was measured from each pressure gage time history. The measurements are summarized in Table 2. No overpressure duration measurement was available for gage 2 in test 2 because a second shock peak was observed before the pressure from the primary shock wave decayed to atmospheric pressure.

**Fig. 8** **a** Original high-speed image and **b** background subtraction image from test 2 showing the anomalous fragment that impacts near the pressure gage prior to the primary shock wave impingement. The shock wave is clearly visible in **a** due to its distortion of the background, and processing is not necessarily required, but is still used to improve the identification of the leading edge. The “smearing” of the shock wave caused by the long exposure image can be observed in **a** to the left of the shock wave leading edge

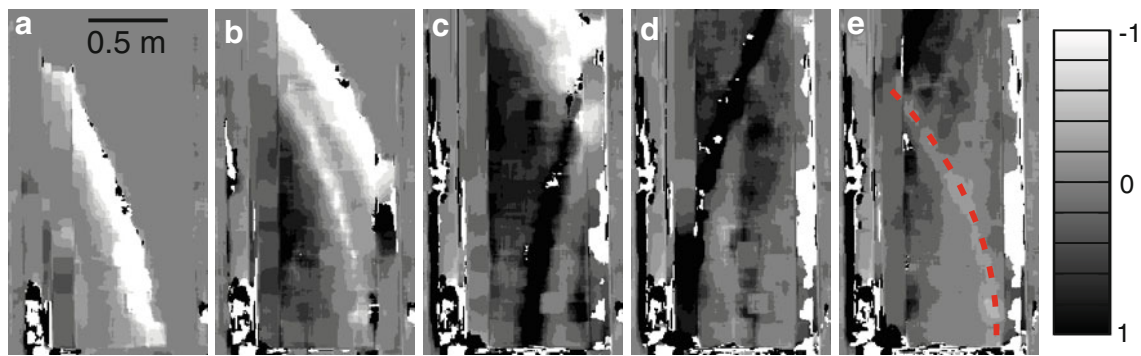


**Fig. 9** Contour images from the image correlation processing of test 1. The image region is the same as shown in Fig. 3b. **a** The primary shock wave propagating from *left to right*, approaching then **(b, c)** reflecting from the wall with the pressure gages. The primary shock then **(d)**

propagates to the *left*, and **(e)** a weaker second shock wave (highlighted with the *dashed line*) approaches the pressure gage wall. The images are  $18 \mu\text{s}$  apart. The contours show horizontal pixel shift from  $-1$  to  $1$  pixels. The plot in **a** is the same as in Fig. 3d

The overpressure duration at each gage was predicted from the shock Mach number versus radius curve [11, 23]. The predicted values, shown in Table 2, have consistently shorter duration than the measured values because the prediction is for the side-on overpressure duration and not the reflected overpressure duration which is measured by the gages. The difference between side-on and reflected overpressure and overpressure duration is measured experimentally and discussed by Rahman et al. [12]. The difference is not significant for test 2, where the scaled distance from the charge center to the gage position is shorter than in test 1. The difference between the reflected and side-on durations is expected to increase with increasing distance from the charge center, due to the larger amount of time that the end of the overpressure duration point will propagate through the reshocked air and against the shocked air velocity. With detailed measurements of the reflected shock wave velocity, the reflected overpressure duration could be predicted. These measurements are outside of the present scope of work, but are being investigated by the author for future publication.

### 3.4 Late-time shock measurement

The pressure gage records in Figs. 6 and 7 show pressure spikes indicating shock wave impacts after the primary shock. From examining only the gage record, it is difficult to determine the origin or nature of these shock wave impacts. The BOS image correlation is used to visualize a second shock wave impact for test 1. This method is required because the primary shock has distorted the test region environment and the simple image subtraction does not clearly distinguish the presence of subsequent shock waves. Figure 9 is a series of contours of measured horizontal pixel shift, calculated in the image region shown in Fig. 3b.

Shock waves propagating from left to right in Fig. 9 are visualized as the white contours because the pixel shift is to

the left (negative). Shock waves propagating from right to left have black contours indicating the opposite pixel shift. The images clearly show the primary shock wave reflecting from the wall and then a second, weaker shock wave approaching the wall. Analysis of the contour images indicates that the second shock impacts pressure gage 1  $t = 0.0167$  s after the charge initiation. This agrees well with the second shock peak in Fig. 6.

This second shock can be tracked in the contour images to determine its Mach number as it impacts the pressure gage location, which can be converted to a peak reflected pressure. This measurement, however, is severely affected by the limited image resolution and inability to identify the shock wave leading edge. This leads to a large experimental uncertainty in the shock Mach number. The second shock wave is less visible in the contour images than the primary shock because the shock wave is weaker in strength and also because the flow image has distortions in it due to the passage of the primary shock which make identifying the second shock more difficult. Determining the local sound speed is also difficult due to the reflected shock flow field. The determination of the peak pressure behind subsequent shock impingements from the optical record is thus left for future research.

Similar measurements were not able to be made in test 2 because the fireball produced by the explosion prevented imaging of the background shortly after passage of the first shock wave.

## 4 Conclusions

Background-oriented schlieren techniques were used to measure shock propagation from C4 explosions. Two analysis techniques were used: an image subtraction method and a correlation method. The techniques were used to measure the shock wave location as a function of time. The back-

ground subtraction method was simpler for this and yielded a higher resolution shock leading edge location; the correlation method tended to yield an uneven shock leading edge. The shock location versus time data was scaled to a 1 kg explosive mass using Sachs' scaling, yielding a single shock radius versus time curve, which was manipulated to yield a Mach number versus radius characterization for C4.

The shock Mach number versus radius curve was used to predict the peak overpressure and overpressure duration at two pressure gage locations. The predictions agreed well with the gage measurements for the peak pressure magnitude and time of arrival. The shock Mach number profile helped to identify a non-ideal fragment impact near a pressure gage, which influenced the recorded pressure. The overpressure duration was measured optically and the results were found to agree with data from pressure measurements within an order of magnitude, but the technique requires further development. The optical measurements contain a relatively large experimental uncertainty due to the camera pixel resolution, but could be improved by limiting the field of view to only the region near the pressure gage.

The correlation-based technique demonstrated the ability to identify multiple shock waves and their propagation direction in a complicated flowfield. This technique would be useful for identifying shock propagation in geometries with multiple shock reflections.

The primary limitation of these techniques was the limited pixel resolution. The image resolution influenced the experimental uncertainty in shock position, velocity, and resulting pressure predictions. The BOS technique also requires a background that is adequately illuminated, which can influence the time resolution available for a test that is illuminated by natural sunlight. The BOS technique also requires a transparent medium to perform visualizations, which for explosives implies that the shock wave has separated from any opaque fireball driving it.

**Acknowledgments** The author would like to acknowledge the support of the personnel at EMRTC, especially R. Weaver, P. Johnston, M. Gerber, G. Walsh, and M. Stanley. This work was partially funded by the Technical Support Working Group (TSWG) under Task PS-3277.

## References

1. Taylor, G.I.: The formation of a blast wave by a very intense explosion 2: the atomic explosion of 1945. *Proc. R. Soc. A* **201**(1065), 175–186 (1950)
2. Dewey, J.M.: The properties of a blast wave obtained from an analysis of the particle trajectories. *Proc. R. Soc. A* **324**(1558), 275–299 (1971)
3. Dewey, J.M.: Expanding spherical shocks (blast waves). In: Bendor, G., Igra, O., Elperin, E. (eds.) *Handbook of Shock Waves*, vol. 2, pp. 441–481. Academic Press, London (2001)
4. Glass, I.I.: Aerodynamics of blasts. *Can. Aeronaut. J.* **7**, 109–135 (1961)
5. Clarke, S., Bolme, C., Murphy, M., Landon, C., Mason, T., Adrian, R., Akinci, A., Martinez, M.: Using schlieren visualization to track detonator performance. *AIP Conf. Proc.* **955**, 1089–1092 (2007)
6. Steward, B.J., Gross, K.C., Perram, G.P.: Optical characterization of large caliber muzzle blast waves. *Propellants Explos. Pyrotech.* **36**, 564–575 (2011)
7. Sommersel, O., Bjerketvedt, D., Christensen, S., Krest, O., Vaagsaether, K.: Application of background oriented schlieren for quantitative measurements of shock waves from explosions. *Shock Waves* **18**, 291–297 (2008)
8. Mizukaki, T., Tsukada, H., Wakabayashi, K., Matsumura, T., Nakayama, Y.: Quantitative visualization of open-air explosions by using background-oriented schlieren with natural background. In: *Proceedings of the 28th International Symposium on Shock Waves*, Manchester, vol. 1, pp. 465–470 (2012)
9. Kleine, H., Dewey, J.M., Ohashi, K., Mizukaki, T., Takayama, K.: Studies of the TNT equivalence of silver azide charges. *Shock Waves* **13**, 123–138 (2003)
10. Kleine, H., Timofeev, E., Takayama, K.: Laboratory-scale blast wave phenomena—optical diagnostics and applications. *Shock Waves* **14**, 343–357 (2005)
11. Hargather, M.J., Settles, G.S.: Optical measurement and scaling of blasts from gram-range explosive charges. *Shock Waves* **17**, 215–223 (2007)
12. Rahman, S., Timofeev, E., Kleine, H.: Pressure measurements in laboratory-scale blast wave flow fields. *Rev. Sci. Instrum.* **78**: 125106 (2007)
13. Meier, G.E.A.: Computerized background-oriented schlieren. *Exp. Fluids* **33**, 181–187 (2002)
14. Dalziel, S.B., Hughes, G.O., Sutherland, B.R.: Synthetic schlieren. In: *Proceedings of the 8th International Symposium on Flow Visualization*, paper 62
15. Richard, H., Raffel, M.: Principle and applications of the background oriented schlieren (BOS) method. *Meas. Sci. Technol.* **12**, 1576–1585 (2001)
16. Hargather, M.J., Settles, G.S.: Natural-background-oriented schlieren. *Exp. Fluids* **48**, 59–68 (2010)
17. Dalziel, S., Hughes, G., Sutherland, B.: Whole-field density measurements by 'synthetic schlieren'. *Exp. Fluids* **28**, 322–335 (2000)
18. Venkatakrishnan, L., Meier, G.E.A.: Density measurements using the background oriented schlieren technique. *Exp. Fluids* **37**, 237–247 (2004)
19. Elsinga, G.E., Oudheusden, B.W.V., Scarano, F., Watt, D.W.: Assessment and application of quantitative schlieren methods: calibrated color schlieren and background oriented schlieren. *Exp. Fluids* **36**, 309–325 (2004)
20. Hargather, M.J., Settles, G.S.: A comparison of three quantitative schlieren techniques. *Opt. Laser Eng.* **50**, 8–17 (2012)
21. Settles, G.S.: *Schlieren and Shadowgraph Techniques: Visualizing Phenomena in Transparent Media*. Springer, Berlin (2001)
22. Menon, D., Calvagno, G.: Color image demosaicking: an overview. *Signal Process. Image Commun.* **26**, 518–533 (2011)
23. Kinney, G.F., Graham, K.J.: *Explosive Shocks in Air*. Springer, Berlin (1985)